Published in final edited form as:
Cell Host Microbe. 2014 May 14; 15(5): 537–550. doi:10.1016/j.chom.2014.04.002.

The *Toxoplasma* pseudokinase ROP5 forms complexes with ROP18 and ROP17 kinases that synergize to control acute virulence in mice

Ronald D. Etheridge[1], **Aditi Alaganan**[1], **Keliang Tang**[1], **Hua Jane Lou**[2], **Benjamin E. Turk**[2], and **L. David Sibley**[1,*]

[1] Department of Molecular Microbiology, Washington Univ. Sch, Med., 660 S. Euclid Ave, St. Louis Mo 63110, USA

[2] Department of Pharmacology, Yale University School of Medicine, 333 Cedar St., New Haven, CT, 06520, USA

Summary

Polymorphic rhoptry secreted kinases (ROPs) are essential virulence factors of *Toxoplasma gondii*. In particular, the pseudokinase ROP5 is the major determinant of acute virulence in mice, but the underlying mechanisms are unclear. We developed a tandem affinity protein tagging and purification approach in *T. gondii* and used it to show that ROP5 complexes with the active kinases ROP18 and ROP17. Biochemical analyses indicates that ROP18 and ROP17 have evolved to target adjacent and essential threonine residues in switch region I of immunity related GTPases (IRGs), a family of host defense molecules that function to control of intracellular pathogens. The combined activities of ROP17 and ROP18 contribute to avoidance of IRG recruitment to the intracellular *T. gondii* containing vacuole, thus protecting the parasite from clearance in interferon-activated macrophages. These studies reveal an intricate, multi-layered parasite survival strategy involving pseudokinases that regulate multiple active kinase complexes to synergistically thwart innate immunity.

Introduction

Toxoplasma gondii is a widespread parasite that infects warm-blooded vertebrates, leading to zoonotic infections in humans (Dubey, 2010). The majority of isolates in North America and Europe belong to one of three distinct lineages where type I strains are acutely virulent, while type II are intermediate, and type III are avirulent in the laboratory mouse (Sibley and Ajioka, 2008). The ability to cross strains in the cat was exploited to develop forward genetic strategies to map genes controlling differences in acute virulence (Khan et al., 2005; Su et al., 2002). Quantitative trait locus (QTL) mapping identified the active rhoptry kinase ROP18 as the major determinant of the difference between highly virulent type I and

* Corresponding author: sibley@wustl.edu, TEL: 314-362-8873, FAX: 314-286-0060.

avirulent type III parasites (Taylor et al., 2006), and between intermediate virulence type II parasites and avirulent type III parasites (Saeij et al., 2006). ROP18 has several targets in the host cell, including immunity related GTPases (IRGs) (Fentress and Sibley, 2011) that function in innate immunity, and ATF6β (Yamamoto et al., 2011), a component of the unfolded protein response that influences adaptive immunity. IRGs are strongly induced by IFN-γ and are important in cell-autonomous restriction of *T. gondii* and other intracellular pathogens (Taylor et al., 2007). Preferential recruitment of IRGs to the nascent parasitophorous vacuole membrane (PVM) surrounding susceptible strains of *T. gondii* leads to disruption of the vacuole and parasite death (Khaminets et al., 2010; Zhao et al., 2009). ROP18 from type I strains is able to phosphorylate specific threonine residues in switch region I of the GTPase domain of IRGs and this modification is likely responsible for inactivating the GTPase function, thus preventing oligomerization and loading on the PVM (Fentress et al., 2010; Steinfeldt et al., 2010). Although ROP18 from both type I and type II strains are capable of enhancing virulence when expressed in a type III background, which is normally hypomorphic for ROP18 expression, type II strains are nonetheless susceptible to IRG recruitment (Khaminets et al., 2010; Zhao et al., 2009), indicating that additional genes shared by type I and III strains are important for acute virulence.

Forward genetic mapping of virulence differences between strain types I × II and II × III identified a major virulence locus encoding the pseudokinase ROP5 (Behnke et al., 2011; Reese et al., 2011). Type I and III strains share a similar complement of *ROP5* alleles that are necessary for acute virulence, while type II strains contain a distinct cluster of *ROP5* alleles that is associated with lower virulence (Behnke et al., 2011; Reese et al., 2011). The major type I allele of ROP5 interacts with IRGs (Fleckenstein et al., 2012), and increases the kinase activity of ROP18 (Behnke et al., 2012), consistent with the genetic evidence that these two factors work together to enhance virulence. However, the large phenotypic differences between the type I Δ*rop18* mutant, which is only slightly attenuated (Fentress et al., 2010), *vs.* the Δ*rop5* mutant, which is completely avirulent even at high doses (Behnke et al., 2011; Reese et al., 2011), suggests that ROP5 also has other functions.

Here we explored alternative roles for ROP5 using a biochemical approach to identify binding partners by tandem affinity purification (TAP) tagging and mass spectrometry (MS). Our findings reveal that ROP5 is found in complexes together with ROP18 and an unrelated, but active kinase called ROP17, which together mediate protection from the IRG pathway.

Results

Purification of rhoptry kinase complexes

To identify binding partners of ROP5, we developed a tandem affinity purification (TAP) strategy to isolate native complexes from *T. gondii* tachyzoites. We engineered a *T. gondii* cell line constitutively expressing a Tet-repressor-YFP fusion protein (van Poppel et al., 2006), to provide a background for introducing Tet-inducible expression constructs (Figure 1A). The major type I allele of ROP5 (H-allele) (Behnke et al., 2011) was expressed as a TAP-tag fusion with a calmodulin binding peptide and a protein A moiety (Puig et al., 2001). Over-expression of the TAP-tagged ROP5 was induced with tetracycline (Tet) (Figure 1B). Purification of the ROP5 complex (Figure 1C) and subsequent mass

spectrometry (MS) analysis identified approximately 15 proteins each with at least 5 unique peptides (Table1). The ROP5-TAP complex included the previously characterized active kinase ROP18, as well as an uncharacterized ROP kinase called ROP17, which was initially described as a component of purified rhoptries (Bradley et al., 2005), (Table 1). Other prominent components included a S/T phosphatase, ROP pseudokinases such as ROP2/8 and ROP4/7, as well as a variety of other proteins (Table 1). Additional proteins lacking predicted signal peptides were not studied further, since ROP5 is present in the secretory pathway (Table S1).

To validate the associations between ROP kinases and ROP5, we performed reciprocal TAP-purification of both ROP18 and ROP17 TAP-tagged lines (Figure 1B). Analysis of ROP18-TAP complex (Figure 1C middle panel) confirmed binding with ROP5 and also detected peptides for ROP17, albeit to a lesser extent (Table 1). The ROP17-TAP (Figure 1C right panel) also validated the association of ROP5, although this complex did not contain ROP18 (Table 1). GRA7, which also immunoprecipitates (IP) with ROP18 (Alaganan et al., 2013; Dunn et al., 2008), was also seen in the ROP5 and ROP18 complexes, although not in the ROP17 complex (Table 1). Additionally, all three TAP purifications contained a SMC domain containing protein, predicted to be a component of chromatin modifying complexes, Hsp70, a chaperone involved in protein folding, and a cyst matrix protein, which is a component of the matrix of tissue cysts that is upregulated in bradyzoites (Parmley et al., 1994). Given their diverse functions and lack of obvious connection with the interface at the PVM, these later proteins may simply represent co-purifying contaminants and they were not pursued further here (Table 1).

To further characterize the ROP kinase complexes, we subjected whole cell parasite extracts to sedimentation on 10-30% glycerol gradients followed by SDS-PAGE and Western blotting (Figure 2A). ROP5, ROP17, and ROP18 sedimented broadly in the ~4-20 S range, suggesting that they comprise a variety of high molecular weight complexes. ROP18 has previously been extensively studied (Fentress and Sibley, 2011), while ROP17 has not yet been examined for its role in intracellular survival or acute virulence. Hence, we focused our studies on defining the role of ROP17 as a binding partner of ROP5.

ROP17 and ROP5 are secreted in evacuoles and localized to the external face of the PVM

Similar to other ROP2 family members, ROP17 contains an N-terminal amphipathic region that targets heterologous reporters to the PVM (Reese and Boothroyd, 2009). To examine the location of endogenous ROP17, human foreskin fibroblast (HFF) monolayers were infected with *T. gondii* in the presence of cytochalasin D, which blocks invasion but allows secretion of rhoptry contents in evacuoles into the host cell (Håkansson et al., 2001). Both ROP17 and ROP5 were found in secreted evacuoles by immunofluorescence (IF) microscopy (Figure 2B). In cells that were selectively permeablized with digitonin, ROP5 and ROP17 were found to co-localize on the cytosolic surface of newly formed vacuoles (Figure 2C), a pattern that was maintained for up to 16 hours post-infection (Figure 2D). Under these selectively permeable conditions, ROP17 stained the PVM while the parasite surface antigen (SAG1) was not detectable (Figure S1A-B). The localization of ROP17 to the parasite vacuole external face was not dependent on the presence of ROP5 as vacuoles

surrounding RHΔ*rop5* parasites had a normal distribution of ROP17 (Figure S1C-D). In fully permeabilized cells examined at later stages of infection, dividing parasites showed clear co-localization of ROP17 and ROP5 within apical rhoptry organelles (Figure 2E). Collectively these data suggest that ROP5 and ROP17 are found in a complex that localizes to the external face of the PV.

ROP17 is under positive selection and its native complex displays robust kinase activity

Phylogenic analysis of ROP17 in representative strain types I, II, and III, revealed the presence of a shared allele in the type II and III lineages that differed at 24 amino acids from that found in type I (Figure 3A). Examination of the cumulative differences in synonymous (S) and nonsynonymous (NS) mutations in the two alleles of ROP17 (Figure 3B) demonstrated a pNS/pS ratio of 1.50 (Figure 3C). Hence, ROP17 is polymorphic and under positive selective pressure, albeit to a lesser extent than either ROP18 or ROP5 (Peixoto et al., 2010).

ROP17 contains a conserved catalytic triad that predicts it to be an active S/T protein kinase (Hanks and Hunter, 1995). We compared the isolated ROP17-TAP and ROP5-TAP complexes to recombinant ROP17 (rROP17) using an *in vitro* kinase reaction in the presence of ^{32}P-γ -ATP and the heterologous substrate casein. The ROP5-TAP complex showed strong activity (Figure 3D), with a result likely due to its interaction with both ROP18 and ROP17, since ROP5 lacks demonstrable activity when expressed alone as a recombinant protein (Behnke et al., 2012; Reese and Boothroyd, 2011). The activity of the native ROP17-TAP complex was far greater than rROP17 alone (Figure 3D), suggesting that additional factors present in the complex *in vivo* contribute to its activity. To determine if ROP5 was required for the activity of ROP17, we immunoprecipitated ROP17 from wild type (Δ*ku80*) *T. gondii* lysates, as well as from several deletion mutant lines. Precipitated ROP17 complexes were subjected to an *in vitro* kinase reaction in the presence of the synthetic substrate dMBP (Figure 3E) or the IRG protein Irgb6 (Figure 3F). Although the activity of ROP17 was absent in the Δ*rop17* background, ROP17 did not require the presence of ROP5 for activity *in vitro*.

ROP17 contributes to virulence of type I parasites

Based on the finding that ROP5 is found in complexes with ROP17, we hypothesized that one contribution of ROP5 to acute virulence might be due to of its interactions with ROP17. We generated a Δ*rop17* deletion mutant that was confirmed by diagnostic PCR (Figure S2A) and Western blotting in comparison with Δ*rop18* and Δ*rop5* mutants described above (Figure 4A). Inoculation of CD1 mice with 100 Δ*rop17 T. gondii* parasites resulted in slight attenuation of virulence relative to the parental control (Δ*ku80*) (Figure 4B). To address the possibility that ROP17 and ROP18 might be partially redundant, we deleted *ROP18* in the Δ*rop17* background (Figure 4A, S2A-C). Unlike either of the single mutants, the Δ*rop17*Δ*rop18* mutant was completely avirulent in mice at a dose of 100 parasites (Figure 4B). To examine the magnitude of parasite attenuation in the Δ*rop17*Δ*rop18* line we infected CD1 mice with increasing doses of parasites, establishing that this mutant has an LD_{50} of ~ 10^6, a > 4-log increase over the single knockout mutants (Figure 4C). Various attempts to complement the *ROP17* gene in this background proved unsuccessful and

therefore, we generated the double deletion mutant in the reverse order by deleting *ROP17* on the previously generated Δ*rop18* background (Figure S2D). Two independent double Δ*rop18*Δ*rop17* mutants recapitulated the decreased virulence of original Δ*rop17*Δ*rop18* mutant in the mouse (Figure S2E-F).

Attenuation of Δ*rop17* parasites is due to greater immunological control

To test whether the virulence defect of the Δ*rop17*Δ*rop18* mutant was due to increased susceptibility to immune control, we infected Ifnγr$^{-/-}$ mice and monitored survival. Infection of Ifnγr$^{-/-}$ mice with Δ*rop17*Δ*rop18* parasites resulted in 100% mortality by 10 days post infection, while C57BL/6 control mice survived (Figure 5A). Consistent with a requirement for T-cell mediated IFN-γ production, Rag1$^{-/-}$ mice were susceptible to challenge with Δ*rop17*Δ*rop18*, albeit with a slightly delayed death phenotype relative to wild type *T. gondii* (Δ*ku80*) (Figure S3A). In contrast, X-CGD$^{-/-}$ mice, which are deficient in the phagocyte oxidase-mediated respiratory burst (Pollock et al., 1995), showed no change in the attenuation of the Δ*rop17*Δ*rop18* mutant (Figure S3B). Nos2$^{-/-}$ mice, which are deficient in reactive nitrogen generation (MacMicking et al., 1995), displayed an intermediate phenotype characterized by delayed death associated with late stage neurological disease, likely due to an inability to control low level infection in the brain (Figure S3C-F). All of mutants showed similar levels of replication in macrophages activated only with IFN-γ and greater control of replication (stasis) in macrophages activated with both IFN-γ and LPS (Figure S3G), suggesting they are not differentially sensitive to NO. Taken together, these findings indicate that the attenuation of Δ*rop17*Δ*rop18* mutants is due to an inability to effectively thwart IFN-γ-mediated innate immune defenses, rather than an inability of parasites to grow within the host.

Resistance to the host IRG pathway is partially mediated by ROP17

The primary mechanism of IFN-γ mediated control of *T. gondii* in the mouse is due to upregulation of IRGs, which are recruited to susceptible parasite-containing vacuoles that are subsequently destroyed (Howard et al., 2011). To evaluate the role of this pathway, we infected IrgM3$^{-/-}$ mice with the Δ*rop17*Δ*rop18* mutant (Figure 5B). We observed a complete reversion to virulence in the IrgM3$^{-/-}$ mice (Figure 5B) suggesting that ROP17 may also operate in this pathway. To determine if the attenuation of the single Δ*rop17* mutant and the Δ*rop17*Δ*rop18* mutant was due to enhanced susceptibility to IRG-mediated clearance, RAW 264.7 mouse macrophages were activated with IFN-γ and LPS and examined for the ability to clear parasite infection during the first 20 hr post-infection. Parasites deficient in ROP17 showed a significant increase in susceptibility to clearance by IFN-γ-activated macrophages relative to wild type parasites and this deficiency was significantly increased in the double deletion mutant (Figure 5C). To determine if clearance was IRG-mediated, we examined the loading of Irga6 and Irgb6 on the PVM in activated macrophages infected with wild type and mutant parasites. Although deletion of *rop17* alone resulted in only a modest increase in loading of IRGs, Δ*rop17*Δ*rop18* parasites showed significantly increased loading of Irgb6 and Irga6 (Figure 5D-G). Similar results were obtained when we quantified the intensity of Irgb6 and Irga6 loading onto the PVM surrounding parasites (Figure S4A-B). In addition, similar levels of IRG loading were observed at 2 hr post-infection (Figure S4C-D). Collectively these findings indicate that both

ROP17 and ROP18 contribute to the resistance of *T. gondii* to clearance by the IRG pathway.

ROP17 phosphorylates a conserved motif in SWI of IRGs and inhibits IRG polymerization

To determine the substrate preference for ROP17, we performed an *in vitro* kinase assay using a positional-scanning peptide array (Turk et al., 2006). Similar to ROP18 (Fentress et al., 2010), ROP17 showed a strong preference for Thr over Ser as the target of phosphorylation (Figure 6A). Using the phosphorylation intensity data from the peptide array, we generated a probability matrix motif for ROP17, which revealed a slight preference for hydrophobic residues surrounding the phosphorylation site (Figure 6B). We then used the probability matrix to define preferred Thr-containing motifs within the family of mouse IRGs and the top scoring motifs were used to generate MEMEs for ROP17 and ROP18. The highest scoring match corresponded to a highly conserved site within switch region I (SWI), where the preferred ROP17 motif was centered on Thr102, while the ROP18 motif was centered on Thr108 (Figure 6C). The preference of ROP17 for Thr102 and ROP18 for Thr108 was predicted for numerous members of the IRG family (Figure S5A). In order to test the target prediction, we performed an *in vitro* kinase assay on recombinant Irgb6 and Irga6 with and without the addition of ROP5. We observed that ROP17 prefers Irgb6 as a substrate and that, in contrast to what was observed for ROP18 (Behnke et al., 2012), the activity of ROP17 was unaltered by the addition of ROP5 (Figure 6D). MS analysis of the ROP17 phosphorylated Irgb6 protein revealed that the only high confidence phosphorylation site corresponded to Thr102, as predicted by the motif analysis (Figure 6E). Semi-quantitative MS analysis demonstrated a greater than 8-fold relative preference for Thr102 over Thr107, while phosphorylation of Thr108 was not observed (Figure 6F, S5B-E).

To examine whether phosphorylation of Irgb6 by ROP17 affected its ability to form higher order polymers, we combined Irgb6 in the presence of GTP with increasing amounts of rROP17 protein and analyzed the products by Native-PAGE gel followed by Western blotting (Figure 6G). We observed that Irgb6 incubated without GTP formed primarily monomers, dimers, and tetramers (Figure 6G). In contrast, in the presence of GTP, Irgb6 formed large polymers over 720 kDa, which were more evident on overexposure (Figure 6G right panel). Addition of increasing amounts of ROP17 to the reaction resulted in a concomitant decrease in the amount of Irgb6 polymer (Figure 6G). Probing Native Western blots with an anti-phospho-threonine antibody demonstrated that large oligomers of Irgb6 comprise the major phosphorylated form despite being less abundant (Figure 6H). ROP17 was not incorporated into the high molecular weight oligomeric forms of Irgb6 (Fig S6A) and therefore likely does not contribute significantly to this phosphorylation signal, despite being able to auto-phosphorylate (Figure 6D). At the highest concentration of ROP17 tested, phosphorylated monomers and dimers accumulated, likely as a result of disassembly of phosphorylated polymers (Figure 6GH). Additionally, the loss of the Irgb6 oligomeric forms in the presence of ROP17 was observed in glycerol gradients (Figure S6B). These results suggest that the preferred substrate for ROP17 is the Irgb6 polymer and that phosphorylation leads to disassembly into monomers and dimers.

Discussion

We utilized TAP-tagging of proteins in *T. gondii* to demonstrate that the pseudokinase ROP5 exists in complexes with two active S/T kinases: ROP18, previously known from genetic interaction studies, and ROP17, a virulence factor identified in this study. ROP17 also targets members of the IRG family to prevent clearance in IFN-γ-activated macrophages, thus providing a cellular basis for its synergy with ROP18. The substrate preferences of these two kinases are tailored to target two conserved residues in SWI that are essential for IRG function. Moreover, unlike previous mechanisms that have been proposed for IRG disruption, ROP17 targets IRG oligomers, leading to their disassembly, a process that may contribute to protection of the PVM in infected macrophages. Taken together, our findings reveal that *T. gondii* has evolved a multilayered system of effectors to specifically target the diverse array of IRGs encountered in IFN-γ activated cells, thereby thwarting innate immunity.

TAP-tagging has been a useful strategy for identifying complexes in a variety of organisms (Puig et al., 2001), and therefore we undertook the development of this technology in *T. gondii.* TAP-tagging of ROP5 demonstrated that it exists in two distinct complexes each containing predominately ROP18 or ROP17, as well as related ROP pseudokinases ROP2/8 and ROP4/7. It is uncertain what role these pseudokinases play in the complexes studied here, although deletion of the *ROP2/8* or *ROP4/7* loci does not affect acute virulence in the mouse ((Alaganan et al., 2013) and unpublished data). GRA7 was also found in the complex with ROP18, consistent with the recent report that it acts synergistically to affect IRG recruitment and virulence (Alaganan et al., 2013). The migration of ROP5, ROP17, and ROP18 on gradients suggests that they are components of heterogeneous complexes of various compositions. Further work will be required to define the exact composition of these complexes in the secretory pathway and on the PVM, where they co-exist.

ROP kinases are expanded in the genome of *T. gondii* with ~20 genes that are predicted to encode active kinases and a similar number predicted to encode pseudokinases (Peixoto et al., 2010). *ROP18* is a member of the sub-group known as ROP2-like genes, while *ROP17* is more divergent, as shown by comparison of their kinase domains (Peixoto et al., 2010). Despite this divergence, ROP17 and ROP18 target a common pathway in the host by phosphorylating members of the IRG family. Consistent with their overlapping functions, single deletion of either gene only had a modest effect on virulence, characterized by a delayed time to death, but nonetheless a lethal outcome even with low inocula (present data and (Fentress et al., 2010)). In contrast, the Δ*rop17rop18* mutant has an LD_{50} of ~10^6, which is more severely attenuated yet still not as compromised as the Δ*rop5* mutant (Behnke et al., 2011; Reese et al., 2011). Although previous studies have suggested that the Δ*rop5* mutant does not persist in wild type mice (Behnke et al., 2012), we observed increased CNS pathology in mice infect with the double Δ*rop17*Δ*rop18* mutant, consistent with an increase capacity to disseminate and cause low-grade infection. Importantly, the phenotypes of all three mutants are completely reverted in Ifnγr1$^{-/-}$ mice, which cannot signal in response to IFN-γ (Yap and Sher, 1999), and in IrgM3$^{-/-}$ mice, which lack a functional IRG pathway (Taylor et al., 2000). Thus, although ROP5 and ROP17 may have other targets beyond IRGs, avoidance of this early innate pathway is one of their critical functions.

Previous studies indicate that the primary mechanism that IFN-γ activated cells in the mouse use to control *T. gondii* is upregulation of the IRG pathway (Howard et al., 2011). Together with ROP18 (Behnke et al., 2011; Reese et al., 2011) and ROP5 (Behnke et al., 2011; Reese et al., 2011), our findings indicate that ROP17 works collectively to block the IRG pathway. This triad of virulence effectors is most effective in type I parasites, which contain a highly expressed *ROP18* and virulence-enhancing *ROP5* locus, while type II strains have an active *ROP18* but avirulent *ROP5* locus (Hunter and Sibley, 2012). Importantly, type III strains are completely avirulent, despite having the virulence-enhancing *ROP5* locus, which is ineffective in the absence of highly expressed *ROP18* (Hunter and Sibley, 2012). Although ROP17 participates in acute virulence, previous genetic mapping studies failed to reveal a QTL for this locus, even though it is polymorphic with type II and III strains sharing an allele that is distinct from type I. Further genetic and biochemical studies may clarify whether ROP17 alleles act differently in combination with ROP18 and/or ROP5.

Consistent with the fact that ROP17 and ROP18 act synergistically to affect acute virulence, they target slightly different conserved residues in a common set of host targets. In both cases, they show a preference for phosphorylating SWI within the GTPase domain of IRGs. We show that ROP17 shows a preference *in vitro* for Irgb6 over Irga6, while previous studies indicate that ROP18 prefers Irga6 (Steinfeldt et al., 2010), although it also phosphorylates both Irgb6 and Irgb10 albeit less avidly (Fentress et al., 2010). Despite these *in vitro* preferences, increased recruitment of both Irgb6 and Irga6 was seen in either single mutant suggesting that substrate preferences may be modulated *in vivo* or that these host proteins work together in complexes. ROP18 was previously shown to phosphorylate multiple Thr residues in SWI of Irga6 (Thr102, Thr108) (Steinfeldt et al., 2010), as well as in Irgb6 (Thr102, Thr107, Thr108) (Fentress et al., 2010); however, no quantitative assessment of the relative preference for phosphorylation of these residues was provided. In the present study, we re-examined the substrate preference motifs for both kinases revealing that ROP17 prefers to phosphorylate Thr102, while ROP18 prefers Thr108. We confirmed that ROP17 prefers Thr102 over Thr108 in Irgb6 using a semi-quantitative MS approach, thus validating this prediction for at least one substrate. These two Thr residues are conserved in many IRG family members yet they are distinct from SWI of other small GTPases, suggesting these kinases have evolved to specifically target IRGs. Previous mutational studies demonstrated that Thr102 and Thr108 are essential for GTPase activity and oliogomerization of Irga6 (Steinfeldt et al., 2010), suggesting that phosphorylation of these residues renders the protein inactive. Hence, the activities of ROP17 and ROP18 should combine to phosphorylate IRGs on key Thr residues, blocking their oligomerization and preventing assembly on the PVM. Consistent with this prediction, the single Δ*rop17* and Δ*rop18* mutants show increased IRG recruitment in IFN-γ activated macrophages, and recruitment is further enhanced in the Δ*rop17rop18* mutant.

Previous studies have stressed the role of ROP5 in blocking IRG oligomerization *in vitro* as detected by light scattering, suggesting a non-catalytic role for ROP5 in sequestering IRGs (Fleckenstein et al., 2012). Additionally ROP5 was shown to enhance the phosphorylation of IRGs by regulating ROP18 (Behnke et al., 2012). Collectively these activities are thought to contribute to avoidance of IRG recruitment to the PVM. However, both of these models

postulate interactions between parasite effectors and monomeric IRGs, which normally only exist in complex with IRGM proteins on endomembranes (Howard et al., 2011). In contrast, IRGs oligomerize and assemble on the PVM owing to the absence of regulatory IRGM proteins, leading to destruction of the invading pathogen (Haldar et al., 2013). The activity of ROP17 is particularly interesting in this light as it is shown to preferentially target IRG polymers. Native gel analysis indicates that ROP17 prefers to phosphorylate IRG oligomers and results in their disassembly, perhaps making monomers available for ROP5 and/or ROP18 to act on further. In this regard, it is intriguing that recent studies have shown that GRA7 can activate IRG assembly *in vitro*, leading to its rapid depolymerization, an effect that may also make monomeric substrates available to ROP5 and ROP18 (Alaganan et al., 2013). Unlike ROP18, ROP17 does not appear to rely on ROP5 for its activity *in vitro.* However, the formation of complexes between ROP5 and ROP17 may facilitate recruitment of substrates or enhance activity *in vivo* to improve the efficiency of combating the IRG pathway.

Our findings reveal an intricate interaction between a multi-component innate defense system that encodes the divergent and amplified IRG genes in the mouse and an expanded family of virulence promoting secretory proteins in the parasite *T. gondii*. These virulence effectors consist of both active and pseudokinases that operate in complexes at the host-parasite interface on the surface of the PVM. The heterogeneous nature of the ROP complexes is presently not fully understood, but their various different states may be involved in regulation, substrate recruitment, and/or target specificity. The amplification of these parallel systems likely reflects the co-evolving relationship between *T. gondii* and the mouse as an important host for transmission. Curiously, for most of the active kinases in *T. gondii*, there is no overt phenotype for single gene deletion mutants when tested in the mouse (unpublished). Instead, the tripartite group of ROP5 ROP18 and ROP17 appear to control the major outcome of acute infection the mouse. This pattern suggests that other ROPs either have redundant and overlapping functions or that they are important in other contexts such as manipulating the many other hosts of *T. gondii*. Hence, the remarkable complexity of host innate defense and pathogen virulence traits revealed here is likely to be mirrored in other settings where this highly successful parasite has established a niche.

One potential example of other roles for ROP kinases would be additional host defense pathways such as guanylate binding proteins (GBPs). Although IRGs are not widely distributed outside of rodents, and are almost absent in humans, the related GBP family is found more widely (Kim et al., 2012). GBPs have been implicated in host resistance to a number of pathogens in the mouse (MacMicking, 2012), including *T. gondii* (Degrandi et al., 2013; Selleck et al., 2013; Yamamoto et al., 2012). Whether they prove to be important in innate immunity in other hosts, and if they are targets of intervention by ROP kinases, will be the subject of future studies.

Experimental Procedures

Parasite growth and mouse infections

Animals were maintained in an Association for Assessment and Accreditation of Laboratory Animal Care approved facility and the Institutional Care Committee at Washington

University in St. Louis, School of Medicine, approved all protocols. Tachyzoites of *T. gondii* strains were propagated in human foreskin fibroblasts and purified as described previously (Fentress et al., 2010). Knockout mutants were generated in the RHΔ*ku80*Δ*hxgprt* strain, as described previously (Behnke et al., 2012; Behnke et al., 2011). Complete lists of parasite strains, primers and plasmids used are found in Table S2-4. Age and sex-matched mice from wild type and knockout backgrounds (see supplementary information) were challenged by intraperitoneal (ip) injection with parasites and cumulative mortality determined at 30 days post injection (Su et al., 2002). Tissues from chronically infected mice were examined microscopically to evaluate histopathology.

In vitro infection studies

The distribution of host and parasite proteins within infected cells was determined by immunofluorescence (IF) staining, as described previously (Fentress et al., 2010) (see supplementary information). Recruitment of host IRGs to the PVM was evaluated at 30 min and 2 hr post-infection, as described previously (Fentress et al., 2010). The distribution of parasite proteins on the PVM was determined using Triton-X-100 to fully permeabilize cells *vs.* digitonin to partially permeabilize infected cells, as described previously (Alaganan et al., 2013). Control of parasite replication in IFN-γ activated RAW cells (150 units/ml IFN-γ, 10 ng/ml LPS) was determined using an in Cell Western protocol (see supplementary information) imaged on the ODYSSEY infrared imager (LICOR Biosciences). Induction of stasis was monitored following infection of IFN-γ activated, alone or in combination with LPS, RAW 264.7 mouse macrophages for 20 hr followed by staining for SAG1 and counting of parasites/vacuole (see supplementary information).

In vitro protein studies

The *ROP17* coding sequence (including amino acids 22-608) (TgGT1_011620) was amplified by genomic DNA from type I RH strain of *T. gondii* using iProof high-fidelity polymerase (Bio-Rad), expressed in *E. coli*, purified and used to generate a polyclonal antisera in mice (see supplementary information). Recombinant ROP5, ROP18, and IRG proteins were purified as described previously (Behnke et al., 2012; Fentress et al., 2010). Immunoprecipitations, Western blotting, and *in vitro* kinase assays were performed as described previously (Behnke et al., 2012; Fentress et al., 2010). The phosphorylation motif for ROP17 was defined as described previously (Fentress et al., 2010; Turk et al., 2006). Whole cell extracts of *T. gondii* were separated on 10-30% linear glycerol gradients centrifuged in a Beckman SW41 rotor at 111,000*g* for 20 hr and analyzed by SDS PAGE. Purified proteins were resolved on 8-16% Native PAGE gels electrophoresed at 4°C for 20 hr at 40 v, followed by Western blotting. Further details are found in the supplementary information.

Generation of inducible TAP-tag system for *T. gondii*

The TAP-tagging approach was adapted from previous methods ((Puig et al., 2001) with modifications as described below. Type I GT1 strain parasites were transfected with a plasmid containing yellow fluorescent protein (YFP) fused to the N-terminus of the *Escherichia coli* Tn10 tet-repressor (TetR) and driven by chloramphenicol selection

(provided by Dick Schaap). Clonal cell lines were isolated and served as the parental lines for the Tet-Inducible TAP-tag system. Plasmids for the inducible TAP-tag system were generated by fusion of a Tet-repressible *T. gondii* RPS13 promoter (van Poppel et al., 2006) to a multiple cloning site (MCS) and followed by an in-frame C-terminal fusion to a calmodulin binding peptide linked to protein A by a TEV cleavage site and containing a Ble selectable marker.

TAP-tagged parasites were grown in mouse L929 cells in RPMI with 5% FBS supplemented with 2 mM L-glutamine and 20 μg/ml gentamicin grown at 37°C in 5% CO2 (complete medium). Following induction, harvested parasites were subjected to sonication in extraction buffer and the lysate was incubated with Fast Flow Agarose-IgG beads (GE Healthcare). The column was treated with TEV protease (Invitrogen) to release the TAP-tagged protein, which was then bound to calmodulin agarose beads (Agilent) in the presence of calcium and eluted with EGTA.

MS Analyses

TAP elution fractions were subjected to proteolysis using trypsin and LysC and peptides were captured using Vivapure C18 microspin columns (Vivascience Corp.). Peptides were analyzed using an LTQ-Orbitrap Velos mass spectrometer (Thermo Fisher Scientific, Rockford, USA) coupled with a nanoLC Ultra (Eksigent, Dublin, USA). Data was processed using Mascot Distiller v2.2 and searched using Mascot Daemon 2.2 (Matrix Science, London, UK). Searches were performed against the *Toxoplasma gondii* database (v6.1) and NCBI nr database (Jan 2011; 12679685 entries).

Statistical Analyses

Statistical analyses were conducted with GraphPad (Prism5) using Student's *t*-tests (2-tailed, unpaired samples, equal variance).

Supplementary Material

Refer to Web version on PubMed Central for supplementary material.

Acknowledgments

We thank Vern Carruthers, Dick Schaap, Ray Hui, Greg Taylor, Herbert Virgin, Mary Dinauer for generously providing reagents and Sebastian Lourido and members of the Sibley lab for many helpful discussions. Histological studies were performed by the Digestive Diseases Research Core Centers at Washington University and slides were analyzed by Suellen Greco, Comparative animal Medicine, Washington University School of Medicine. Mass spectrometry was performed by Sophie Alvarez, Danforth Plant Sciences.

Funding

Supported by grants from the National Institutes of Health (www.nih.gov/) (AI082423, AI036629, P30 DK52574, GM104047). R.D.E. was partially supported by an NRSA award from the National Institutes of Health (F32 AI096853-02). The funders had no role in the study design, data collection, decision to publish, or preparation of the manuscript.

References

Alaganan A, Fentress SJ, Tang K, Wang Q, Sibley LD. Toxoplasma GRA7 effector increases turnover of immunity-related GTPases and contributes to acute virulence in the mouse. Proc Natl Acad Sci (USA). 2013; 111:1126–1131. [PubMed: 24390541]

Behnke MS, Fentress SJ, Mashayekhi M, Li LL, Taylor GA, L.D. S. The polymorphic pseudokinase ROP5 controls virulence in *Toxoplasma gondii* by regulating the active kinase ROP18. PLoS Path. 2012; 8:e1002992.

Behnke MS, Khan A, Wootton JC, Dubey JP, Tang K, Sibley LD. Virulence differences in *Toxoplasma* mediated by amplification of a family of polymorphic pseudokinases. Proc Natl Acad Sci (USA). 2011; 108:9631–9636. [PubMed: 21586633]

Bradley PJ, Ward C, Cheng SJ, Alexander DL, Coller S, Coombs GH, Dunn JD, Ferguson DJ, Sanderson SJ, Wastling JM, et al. Proteomic analysis of rhoptry organelles reveals many novel constituents for host-parasite interactions in T. gondii. J Biol Chem. 2005; 280:34245–34258. [PubMed: 16002398]

Degrandi D, Kravets E, Konermann C, Beuter-Gunia C, Klumpers V, Lahme S, Wischmann E, Mausberg AK, Beer-Hammer S, Pfeffer K. Murine Guanylate Binding Protein 2 (mGBP2) controls Toxoplasma gondii replication. Proc Natl Acad Sci U S A. 2013; 110:294–299. [PubMed: 23248289]

Dubey, JP. Toxoplasmosis of animals and humans. CRC Press; Boca Raton: 2010.

Dunn JD, Ravindran S, Kim SK, Boothroyd JC. The *Toxoplasma gondii* dense granule protein GRA7 is phosphorylated upon invasion and forms an unexpected association with the rhoptry proteins ROP2 and ROP4. Infect Immun. 2008; 76:5853–5861. [PubMed: 18809661]

Fentress SJ, Behnke MS, Dunay IR, Moashayekhi M, Rommereim LM, Fox BA, Bzik DJ, Tayor GA, Turk BE, Lichti CF, et al. Phosphorylation of immunity-related GTPases by a parasite secretory kinase promotes macrophage survival and virulence. Cell Host Microbe. 2010; 16:484–495. [PubMed: 21147463]

Fentress SJ, Sibley LD. The secreted kinase ROP18 defends Toxoplasma's border. Bioessays. 2011; 33:693–700. [PubMed: 21773979]

Fleckenstein MC, Reese ML, Konen-Waisman S, Boothroyd JC, Howard JC, Steinfeldt T. A Toxoplasma gondii Pseudokinase Inhibits Host IRG Resistance Proteins. PLoS Biol. 2012; 10:e1001358. [PubMed: 22802726]

Håkansson S, Charron AJ, Sibley LD. Toxoplasma evacuoles: a two-step process of secretion and fusion forms the parasitophorous vacuole. Embo J. 2001; 20:3132–3144. [PubMed: 11406590]

Haldar AK, Saka HA, Piro AS, Dunn JD, Henry SC, Taylor GA, Frickel EM, Valdivia RH, Coers J. IRG and GBP Host Resistance Factors Target Aberrant, “Non-self” Vacuoles Characterized by the Missing of “Self” IRGM Proteins. PLoS Pathog. 2013; 9:e1003414. [PubMed: 23785284]

Hanks SK, Hunter T. Protein kinases 6. The eukaryotic protein kinase superfamily: kinase (catalytic) domain structure and classification. FASEB Journal. 1995; 9:576–596. [PubMed: 7768349]

Howard JC, Hunn JP, Steinfeldt T. The IRG protein-based resistance mechanism in mice and its relation to virulence in Toxoplasma gondii. Curr Opin Microbiol. 2011; 14:414–421. [PubMed: 21783405]

Hunter CA, Sibley LD. Modulation of innate immunity by Toxoplasma gondii virulence effectors. Nat Rev Microbiol. 2012; 10:766–778. [PubMed: 23070557]

Khaminets A, Hunn JP, Konen-Waisman S, Zhao YO, Preukschat D, Coers J, Boyle JP, Ong YC, Boothroyd JC, Reichmann G, et al. Coordinated loading of IRG resistance GTPases on to the *Toxoplasma gondii* parasitophorous vacuole. Cell Microbiol. 2010; 12:939–961. [PubMed: 20109161]

Khan A, Taylor S, Su C, Mackey AJ, Boyle J, Cole RH, Glover D, Tang K, Paulsen I, Berriman M, et al. Composite genome map and recombination parameters derived from three archetypal lineages of *Toxoplasma gondii*. Nuc Acids Res. 2005; 33:2980–2992.

Kim BH, Shenoy AR, Kumar P, Bradfield CJ, MacMicking JD. IFN-inducible GTPases in host cell defense. Cell Host Microbe. 2012; 12:432–444. [PubMed: 23084913]

MacMicking JD. Interferon-inducible effector mechanisms in cell-autonomous immunity. Nat Rev Immunol. 2012; 12:367–382. [PubMed: 22531325]

MacMicking JD, Nathan C, Hom G, Chartrain N, Fletcher DS, Trumbauer M, Stevens K, Xie QW, Sokol K, Hutchinson N, et al. Altered responses to bacterial infection and endotoxic shock in mice lacking inducible nitric oxide synthase. Cell. 1995; 81:641–650. [PubMed: 7538909]

Parmley SF, Yang S, Harth G, Sibley LD, Sucharczuk A, Remington JS. Molecular characterization of a 65-kilodalton *Toxoplasma gondii* antigen expressed abundantly in the matrix of tissue cysts. Molecular and Biochemical Parasitology. 1994; 66:283–296. [PubMed: 7808478]

Peixoto L, Chen F, Harb OS, Davis PH, Beiting DP, Brownback CS, Ouluguem D, Roos DS. Integrative genomics approaches highlight a family of parasite-specific kinases that regulate host responses. Cell Host Microbe. 2010; 8:208–218. [PubMed: 20709297]

Pollock JD, Williams DA, Gifford MA, Li LL, Du X, Fisherman J, Orkin SH, Doerschuk CM, Dinauer MC. Mouse model of X-linked chronic granulomatous disease, an inherited defect in phagocyte superoxide production. Nat Genet. 1995; 9:202–209. [PubMed: 7719350]

Puig O, Caspary F, Rigaut G, Rutz B, Bouveret E, Bragado-Nilsson E, Wilm M, Seraphin B. The tandem affinity purification (TAP) method: a general procedure of protein complex purification. Methods. 2001; 24:218–229. [PubMed: 11403571]

Reese ML, Boothroyd JC. A helical membrane-binding domain targets the Toxoplasma ROP2 family to the parasitophorous vacuole. Traffic. 2009; 10:1458–1470. [PubMed: 19682324]

Reese ML, Boothroyd JC. A conserved non-canonical motif in the pseudoactive site of the ROP5 pseudokinase domain mediates its effect on Toxoplasma virulence. J Biol Chem. 2011; 286:29366–29375. [PubMed: 21708941]

Reese ML, Zeiner GM, Saeij JP, Boothroyd JC, Boyle JP. Polymorphic family of injected pseudokinases is paramount in Toxoplasma virulence. Proc Natl Acad Sci U S A. 2011; 108:9625–9630. [PubMed: 21436047]

Saeij JPJ, Boyle JP, Coller S, Taylor S, Sibley LD, Brooke-Powell ET, Ajioka JW, Boothroyd JC. Polymorphic secreted kinases are key virulence factors in toxoplasmosis. Science. 2006; 314:1780–1783. [PubMed: 17170306]

Selleck EM, Fentress SJ, Beatty WL, Degrandi D, Pfeffer K, Virgin H.W.t. Macmicking JD, Sibley LD. Guanylate-binding protein 1 (Gbp1) contributes to cell-autonomous immunity against *Toxoplasma gondii*. PLoS Path. 2013; 9:e1003320.

Sibley LD, Ajioka JW. Population structure of *Toxoplasma gondii*: Clonal expansion driven by infrequent recombination and selective sweeps. Ann Rev Microbiol. 2008; 62:329–351. [PubMed: 18544039]

Steinfeldt T, Konen-Waisman S, Tong L, Pawlowski N, Lamkemeyer T, Sibley LD, Hunn JP, Howard JC. Phosphorylation of mouse immunity-related GTPase (IRG) resistance proteins is an evasion strategy for virulent *Toxoplasma gondii*. PLoS Biol. 2010; 8:e1000576. [PubMed: 21203588]

Su C, Howe DK, Dubey JP, Ajioka JW, Sibley LD. Identification of quantitative trait loci controlling acute virulence in *Toxoplasma gondii*. Proc Natl Acad Sci (USA). 2002; 99:10753–10758. [PubMed: 12149482]

Taylor GA, Collazo CM, Yap GS, Nguyen K, Gregorio TA, Taylor LS, Eagleson B, Secrest L, Southon EA, Reid SW, et al. Pathogen-specific loss of host resistance in mice lacking IFN-g-inducible gene IGTP. Proc Nat Acad Sci. 2000; 97:751–755. [PubMed: 10639151]

Taylor GA, Feng CG, Sher A. Control of IFN-gamma-mediated host resistance to intracellular pathogens by immunity-related GTPases (p47 GTPases). Microb Infect. 2007; 9:1644–1651.

Taylor S, Barragan A, Su C, Fux B, Fentress SJ, Tang K, Beatty WL, Haijj EL, Jerome M, Behnke MS, et al. A secreted serine-threonine kinase determines virulence in the eukaryotic pathogen *Toxoplasma gondii*. Science. 2006; 314:1776–1780. [PubMed: 17170305]

Turk BE, Hutti JE, Cantley LC. Determining protein kinase substrate specificity by parallel solution-phase assay of a large number of peptide substrates. Nat Protoc. 2006; 1:375–379. [PubMed: 17406259]

van Poppel NFJ, Welagen J, Duisters RFJJ, Vermeulen AN, Schapp D. Tight control of transcription in *Toxoplasma gondii* using an alternative tet repressor. Int J Parasitol. 2006; 36:443–452. [PubMed: 16516216]

Yamamoto M, Ma JS, Mueller C, Kamiyama N, Saiga H, Kubo E, Kimura T, Okamoto T, Okuyama M, Kayama H, et al. ATF6-beta is a host cellular target of the Toxoplasma gondii virulence factor ROP18. J Exp Med. 2011; 208:1533–1546. [PubMed: 21670204]

Yamamoto M, Okuyama M, Ma JS, Kimura T, Kamiyama N, Saiga H, Ohshima J, Sasai M, Kayama H, Okamoto T, et al. A cluster of Interferon-gamma-inducible p65 GTPases plays a critical role in host defense against Toxoplasma gondii. Immunity. 2012; 37

Yap GS, Sher A. Effector cells of both nonhemopoietic and hemopoietic origin are required for interferon (IFN)-gamma- and tumor necrosis factor (TNF)-alpha- dependent host resistance to the intracellular pathogen, *Toxoplasma gondii*. J Exp Med. 1999; 189:1083–1091. [PubMed: 10190899]

Zhao Y, Ferguson DJ, Wilson DC, Howard JC, Sibley LD, Yap GS. Virulent *Toxoplasma gondii* evade immunity-related GTPas-mediated parasite vacuole disruption within primed macrophages. J Immunol. 2009; 182:3775–3781. [PubMed: 19265156]

Highlights

- The *T. gondii* pseudokinase ROP5 forms complexes with the ROP17 and ROP18 kinases
- ROP17 and ROP18 target distinct threonine residues in host immunity related GTPases (IRGs)
- ROP17 and ROP18 act synergistically to control acute virulence of *T. gondii* in mice
- ROP17 uniquely phosphorylates oligomeric IRGs leading to their disassembly

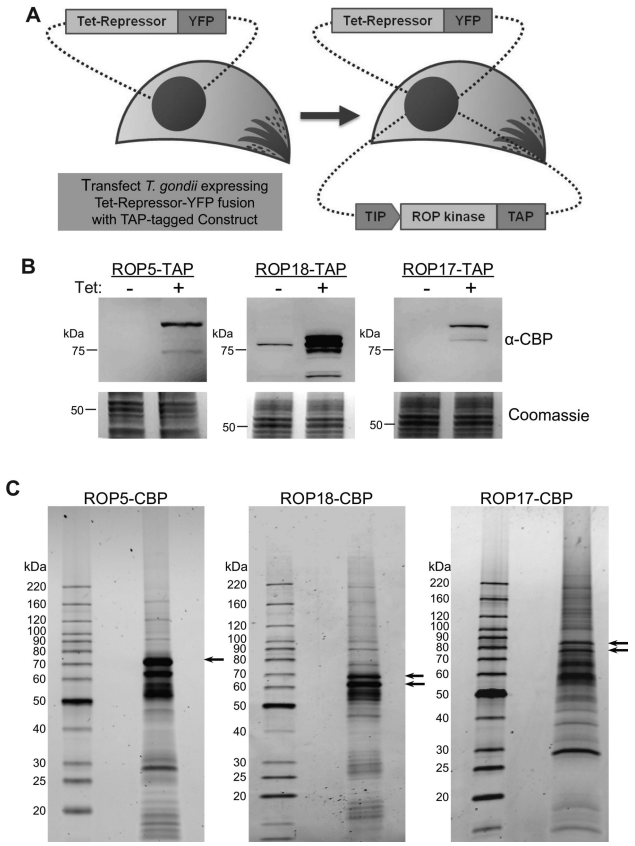

Figure 1. Isolation of rhoptry kinase complexes from *Toxoplasma gondii*

(A) Generation of tetracycline inducible tandem affinity purification (TAP) expression system in *T. gondii*. GT1 strain *T. gondii* cells expressing the tetracycline repressor fused to YFP (Tet-Repressor-YFP) were transfected with plasmid constructs containing rhoptry kinases (ROP) that were C-terminally tagged with calmodulin binding peptide (CBP) and a protein A domain that provides a tandem affinity purification tag (TAP) under the control of a Tet-Inducible Promoter (TIP). (B) Clonal parasite lines expressing ROP5-TAP, ROP18-TAP, or ROP17-TAP were grown in the absence (-) or presence (+) of Tet for 48 hr. Cell extracts were separated on 8-16% SDS-PAGE gels, Western blotted with antibodies against CBP, and imaged using LI-COR specific secondary antibodies. Coomassie stained gels are shown beneath. (C) TAP purifications of rhoptry kinase-CBP complexes. Final elutions were separated on 8-16% SDS-PAGE gels and stained with SYPRO Ruby. Arrows indicate differently processed forms of the tagged rhoptry kinases. Representative of two similar experiments.

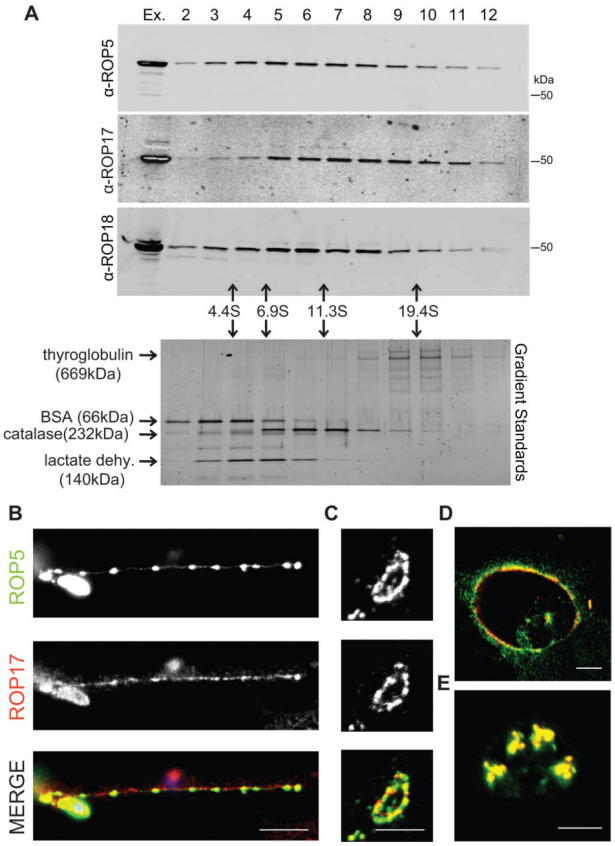

Figure 2. Characterization of the rhoptry kinase complexes

(A) Glycerol gradient separation of ROP kinases. Whole cell extracts of *T. gondii* were fractionated on 10-30% glycerol gradients, resolved on 8-16% SDS-PAGE gels, Western blotted with antibodies shown, and detected using LI-COR specific secondary antibodies. Sedimentation coefficients were determined using standards run in parallel, lower gel stained with SYPRO Ruby. (B) Localization of ROP17 in infected host cells. RHΔ*ku80 T. gondii* parasites were used to challenge HFF monolayers for 30 min in 1μM cytochalasin D to block invasion and visualize proteins secreted into evacuoles. Monolayers were fixed and permeabilized with 0.05% saponin. Alternatively, parasites were allowed to invade HFF cells without cytochalasin D for 30 min (C) or 16 hr (D), fixed, and permeabilized with 0.002% digitonin to selectively expose the cytosolic surface of the PVM. (E) To detect proteins localized to the rhoptries, HFF monolayers were fixed at 16 hr post infection and fully permeabilized with 0.1% TritonX-100. Samples were incubated with mouse anti-ROP17, visualized by goat anti-mouse IgG conjugated to Alexa 594 (red), and rabbit antisera to ROP5, visualized by goat anti-rabbit IgG conjugated to Alexa 488 (green). Scale bars = 5 microns. Representative of two similar experiments. See also Figure S1.

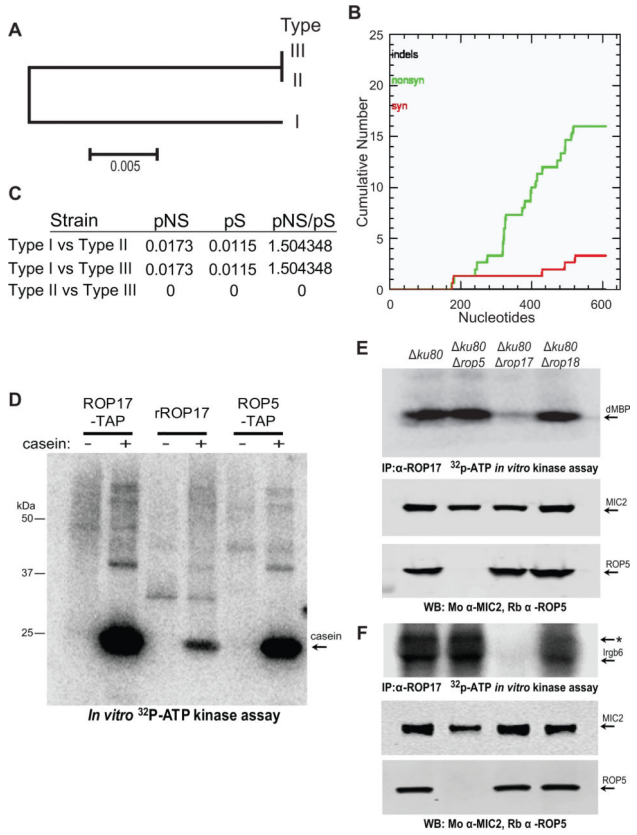

Figure 3. Allelic diversity and kinase activity of ROP17

(A) Phylogenic analysis and neighbor joining tree of ROP17 sequences revealed two alleles in the three clonal lineages (i.e. Types I, II, and III). Scale = substitutions per site. (B) Cumulative nonsynonymous (nonsyn) and synonymous (syn) polymorphisms in *ROP17* genes from A. (C) Proportion of nonsynonymous (pNS) *vs.* synonymous (pS) substitutions for the *ROP17* alleles. (D) Kinase activities of the purified TAP complexes *vs.* rROP17. Casein (20 μg) (arrow) was incubated in a kinase reaction with approximately 2 ng of ROP17-TAP and ROP5-TAP, or alternatively 1 μg of rROP17, for 30 min in the presence of ^{32}P-γ-ATP. Kinase reaction products were resolved on 8-16% SDS-PAGE gels followed by transfer onto nitrocellulose and phosphorimager analysis. (E-F) ROP17 immunoprecipitated (IP) from wild type (Δ*ku80*) or mutant parasite lysates was incubated in a kinase reaction with the heterologous substrate dMBP (E) or Irgb6 (F) in the presence of radiolabelled ^{32}P-γ-ATP. Reaction products were resolved by 8-16% SDS-PAGE followed by transfer to nitrocellulose and phosphorimager analysis. Total parasite lysates were separated on 8-16% SDS-PAGE gels, Western blotted (WB) with mouse anti-MIC2 (Mo α-MIC2) and rabbit anti-ROP5 (Rb α-ROP5), and imaged on the LI-COR Odyssey Imaging System. The * in F likely denotes heavy chain IgG . Representative of three similar experiments.

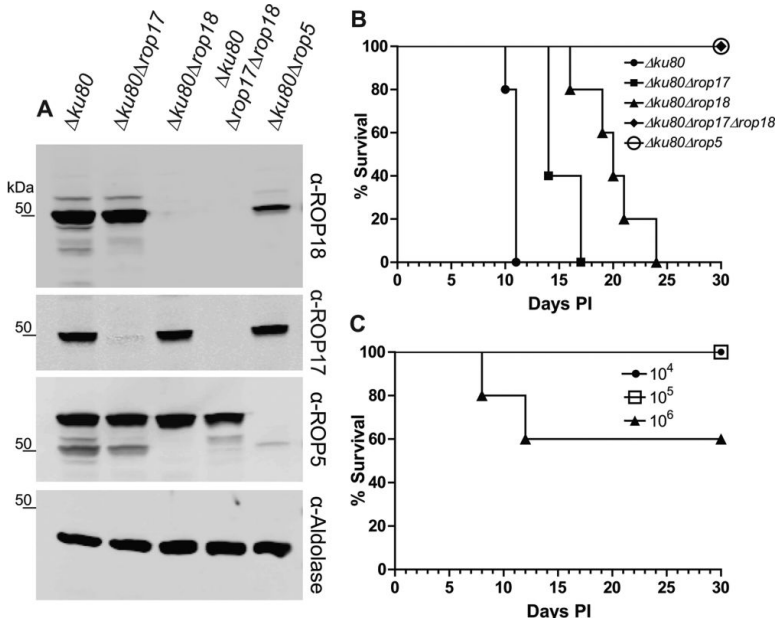

Figure 4. ROP17 and ROP18 act synergistically to control acute virulence in type I parasites

(A) Western blot analysis of deletion mutants. Cell lysates from the wild type (Δ*ku80*) and deletion mutants were separated on 8-16% SDS-PAGE gels, Western blotted with primary antibodies, and imaged on the ODYSSEY imager using LI-COR specific secondary antibodies. (B) Survival of CD-1 mice challenged by ip inoculation with 10^2 wild type (Δ*ku80*) or mutant parasite lines (n = 5 per group). PI, days post-inoculation. (C) Dose response of survival of CD-1 mice challenged by ip inoculation with the double Δ*ku80*Δ*rop18*Δ*rop17* mutant (n = 5 per group). PI, days post-inoculation. Representative of three or more experiments. See also Figure S2.

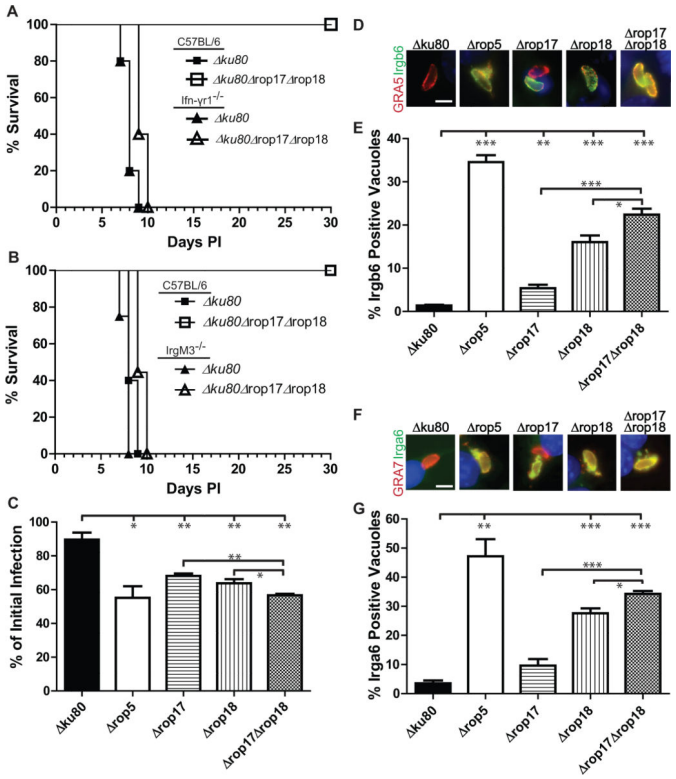

Figure 5. IFN-γ signaling and IRG-mediated clearance is required for control of ROP17 deficient parasites

(A) Survival of Ifnγr1$^{-/-}$ or C57BL/6 mice infected by ip inoculation with 10^3 parasites (n = 5 per group). (B) Survival of IrgM3$^{-/-}$ or C57BL/6 control mice infected by ip challenge with 10^3 parasites (n = 5 per group). (C) *In vitro* clearance of parasites in RAW 264.7 mouse macrophages that were activated with IFN-γ (150 units) and LPS (10 ng/ml). Infection level at 20 hr post-infection expressed as a percentage of initial infection as determined by in-cell Western using the LI-COR ODYSSEY Imaging System. Means ± SEM, n = 3 combined independent experiments. (D-G) Immunofluorescence staining of Irgb6 (D-E) or Irga6 (F-G) on parasite-containing vacuoles in activated (IFN-γ (100 units) and LPS (0.1 ng/ml)) RAW 264.7 mouse macrophages at 30 min post-infection. Scale bar = 5 μm. The percentage of Irgb6 or Irga6 positive vacuoles was determined by comparison to staining with the PVM markers GRA5 or GRA7, respectively. Monolayers were stained with a rabbit polyclonal anti-Irgb6 (green), mAb 10D7 to Irga6 (green), mAb Tg17-113 to GRA5 (red), or rabbit polyclonal anti-GRA7 (red) and detected with Alexa Fluor conjugated secondary antibodies, DAPI (blue). Means ± SEM, n = 3 samples each, from three combined experiments. Student's *t*-test, *$P \leq 0.05$, **$P \leq 0.01$ and ***$P \leq 0.005$. See also Figure S3, S4.

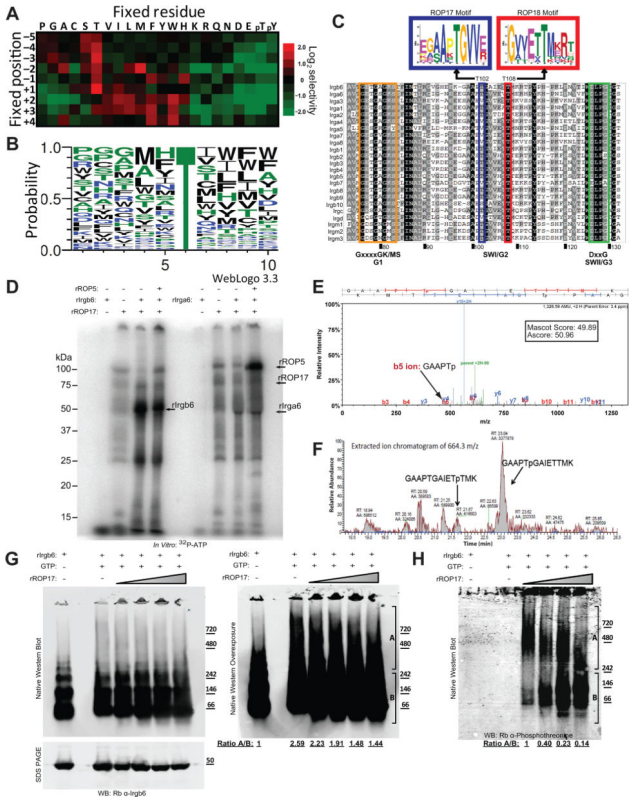

Figure 6. Phosphorylation of IRGs by ROP17 *In vitro*

(A) Phosphopeptide array for *in vitro* ROP17 kinase reaction. For each position (y axis) a single amino acid was held constant (x axis), while all other positions were varied. Phosphoimager analysis of a ^{33}P-γ-ATP kinase reaction was converted into a heat map. Representative of two experiments. (B) Probability matrix for ROP17 determined by WebLogo3.0 from the positional scoring matrix derived from the heat map in (A). (C) MEME sequence motifs for ROP17 and ROP18. Positional scoring matrices were used to determine probable targets within each member of the IRG family using Prophet and the top 5 candidates were used to generate MEME sequence motifs. The top scoring MEMEs for ROP17 and ROP18 are placed above a ClustalX alignment of the IRG family to emphasize the conserved switch region I (SWI) location of their respective predicted phosphorylation sites. (D) *In vitro* kinase activity of rROP17 (1 μg / reaction) on the substrates recombinant Irga6 and Irgb6 (rIrgb6 and rIrga6; 2 μg each) incubated for 40 min at 30°C in the presence of radiolabelled ^{32}P-γ-ATP. Reaction products were separated on 10% SDS-PAGE gels that were dried and imaged by phosphoimager analysis. Representative of two experiments. (E) Mass spectrometry analysis of tryptic peptides derived from *in vitro* phosphorylation of recombinant Irgb6 by rROP17. Representative experiment. (F) Semi-quantitative analysis using LC-MS/MS of phosphorylated peptides of GAAPTGAIETTMK (664.3 m/z ± 15 ppm). (G) Polymerization of Irgb6 following phosphorylation by rROP7 *in vitro*. A kinase reaction combining rROP17 and rIrgb6 in the presence of GTP was carried out for 30 min at 37°C followed by Native-PAGE gel (8-16%) separation and Western blotting for Irgb6. SDS-PAGE followed by Western blotting (lower panel). Right panel is an overexposure of the gel on the left. Irgb6 oligomers (denoted as A) and monomer/dimers (denoted as B) are

shown as ratios at each ROP17 concentration below the gel. (H) The blot in G was re-probed with Rb anti-phosphothreonine antibodies to visualize the phosphorylated proteins. Levels of phosphorylated Irgb6 oligomer (A) and monomer/dimer (B) are shown as ratios below the gel. Western blots were imaged on the ODYSSEY imager using LI-COR specific secondary antibodies. Representative of 3 similar experiments. See also Figure S5, S6.

Table 1

Proteins Identified in Mass Spectrometry Analysis of TAP-purified Rhoptry Complexes.

Protein ID *T. gondii*[a]	Name/Motif	Signal Peptide	ROP5-TAP	ROP18-TAP	ROP17-TAP
TGGT1_042710 [c]	ROP5 (incomplete catalytic triad)	yes	16(136) [b]	20(49)	8(26)
TGGT1_063760 [c]	ROP18	yes	16(49)	34(187)	ND
TGGT1_011620 [c]	ROP17	yes	12(38)	16(24)	12(111)
TGGT1_083640	serine/threonine phosphatase	yes	18(19)	14(14)	ND
TGVEG_030040 [d]	ROP2A (incomplete catalytic triad)	yes	13(43)	14(21)	5(10)
TGGT1_075470	ROP4/7 (incomplete catalytic triad) 2-oxo acid dehydrogenase	yes	13(38)	14(18)	5(10)
TGGT1_062130	acyltransferase	yes	13(16)	16(17)	ND
TGGT1_034740	hypothetical	yes	11(17)	10(13)	ND
TGGT1_072150	SMC domain	yes	10(11)	10(10)	11(25)
TGGT1_108770	cyst matrix protein	yes	10(11)	7(9)	7(38)
TGGT1_087970	heat shock protein 70	yes	10(11)	25(136)	18(23)
TGGT1_017550	GRA7	yes	9(13)	10(17)	ND
TGGT1_088530	hypothetical	yes	6(7)	6(7)	ND
TGGT1_053780	hypothetical	yes	6(7)	7(7)	ND
TGGT1_085550	rhoptry surface protein, putative	yes	5(12)	5(8)	ND
TGGT1_126670	ROP8 (incomplete catalytic triad)	yes	5(7)	19(28)	ND

[a] The cut-off for inclusion of individual proteins into this list was set at five or more unique peptide matches with a probability of 0.95 or above.

[b] Numbers of unique peptides is indicated and those in parenthesis indicate the number of spectra detected for each protein. Proteins lacking a signal peptide were classified as common contaminants (Supplementary Table 1). ND, none detected.

[c] Indicates bait proteins.

[d] Gene models for ROP2A in the GT1 strain were not available. See also Table S1.